ORGANOMETALLICS
Article

Organometallics **2009,** *28,* 5061–5071 5061
DOI: 10.1021/om900345n

Tuning the Efficacy of Ruthenium(II)-Arene (RAPTA) Antitumor Compounds with Fluorinated Arene Ligands

Anna K. Renfrew, Andrew D. Phillips, Enrico Tapavicza, Rosario Scopelliti, Ursula Rothlisberger, and Paul J. Dyson*

Institut des Sciences et Ingénierie Chimiques, Ecole Polytechnique Fédérale de Lausanne (EPFL), CH-1015 Lausanne, Switzerland

Received May 1, 2009

A series of compounds of general formula [Ru(η^6-fluoroarene)(pta)Cl_2] (fluoroarene = C_6H_5F, $C_6H_5CF_3$, and 1,4-$C_6H_4CH_3F$; pta = 1,3,5-triaza-7-phosphatricyclo[3.3.1.1]decane) have been prepared and characterized spectroscopically. Additionally, X-ray diffraction was employed to characterize two of the complexes and the corresponding precursors, i.e., [Ru(acac)$_2$(η^4-cod)] and Ru(η^6-fluoroarene)(η^4-cod)] (cod = cycloocta-1,5-diene). The solubility, pK_a's, and the stability toward hydrolysis of the [Ru(η^6-fluoroarene)(pta)Cl_2] complexes were studied, and DFT calculations were performed to assist in rationalizing the observed properties at a molecular level. The cytotoxicities of the pta-based compounds were evaluated in A2780 ovarian cancer cells, and the observed activities were correlated to the above-mentioned properties. The rate of hydrolysis of the Ru−Cl bonds in the $C_6H_5CF_3$ derivative was found to increase significantly at low pH, which represents a possible method of tumor targeting based on the reduced pH of this particular cellular environment.

Introduction

Ruthenium-based compounds are rapidly gaining interest as potential alternatives to platinum-based chemotherapeutic agents, with some examples having been shown to be effective against cancers not readily treated by cisplatin.[1] In addition, a number of ruthenium-centered complexes have been found to display a significantly higher degree of selectivity toward cancerous cells than the leading commercially available platinum drugs, resulting in reduced damage to healthy tissue. The mechanism of this selectivity is widely debated, but one strong possibility stems from the ability of ruthenium complexes to mimic iron in reversible binding to plasma proteins such as transferrin, which is correlated with the overexpressed concentration of receptors for this protein on the surface of cancer cells. This mechanism provides an effective means for ruthenium complexes to accumulate in cancer cells.[2] Two ruthenium(III)-based drugs, KP1019[3] and NAMI-A,[4] have been shown to bind to the iron(III)-binding sites of transferrin.[5] Moreover, both compounds have recently completed phase I clinical trials and demonstrate a high degree of effectiveness against tumors.

Currently, there is considerable interest in ruthenium(II) compounds as putative anticancer drugs.[6] Part of our work has focused on ruthenium(II)-arene (RAPTA) complexes, which are based on a Ru(II) center with an η^6-coordinated arene, a monodentate P-bound pta ligand, and two chloride ligands, Figure 1, the latter being highly labile depending upon the conditions. *In vitro* studies on various RAPTA complexes (differing by the substitution pattern of the arene ligand) indicate a greater toxicity toward cancer cells than healthy cells, and the corresponding IC_{50} values are relatively high. Moreover, *in vivo*, studies with [Ru(η^6-C_6H_6)(pta)Cl_2], abbreviated RAPTA-B, and [Ru(η^6-*p*-$C_6H_4Me^iPr$)(pta)Cl_2], abbreviated RAPTA-C, revealed a high activity toward metastatic tumors in combination with very low general toxicity.[7]

The selectivity of RAPTA-type complexes toward cancer cells has been proposed to be, at least in part, pH controlled. Tumors generally operate under hypoxic conditions, deriving a significant portion of their energy from glycolysis, resulting in the production of lactic acid, which results in an overall lowering of cellular pH. Tumor cell environments with a pH as low as 5.5 have been reported, in comparison to values of pH 7.2 typically associated with healthy cells.[8]

The notion that RAPTA compounds could display pH-dependent activity stemmed from the observation that

*Corresponding author. E-mail: paul.dyson@epfl.ch.

(1) (a) Kostova, I. *Curr. Med. Chem.* **2006**, *13*, 1085–1107. (b) Galanski, M.; Arion, V. B.; Jakupec, M. A.; Keppler, B. K. *Curr. Pharm. Des.* **2003**, *9*, 2078–2089.
(2) Dyson, P. J.; Sava, G. *Dalton Trans.* **2006**, 1929–1933.
(3) Smith, C. A.; Sutherland-Smith, A. J.; Keppler, B. K.; Kratz, F.; Baker, E. N. *J. Biol. Inorg. Chem.* **1996**, *1*, 424–431.
(4) Alessio, E.; Mestroni, G.; Bergamo, A.; Sava, G. *Curr. Top. Med. Chem.* **2004**, *4*, 1525–1535.
(5) Groessl, M.; Hartinger, C. G.; Egger, A.; Keppler, B. K. *Metal Ions Biol. Med.* **2006**, *9*, 111–116.
(6) (a) Melchart, M.; Sadler, P. J. In *Bioorganometallics*; Jaouen, G., Ed.; Wiley-VCH: Weinheim, 2006; pp 39−62. (b) Ang, W. H.; Dyson, P. J. *Eur. J. Inorg. Chem.* **2006**, *20*, 4003–4018.
(7) Scolaro, C.; Bergamo, A.; Brescacin, L.; Delfino, R.; Cocchietto, M.; Laurenczy, G.; Geldbach, T. J.; Sava, G.; Dyson, P. J. *J. Med. Chem.* **2005**, *48*, 4161–4171.
(8) Gerweck, L. E. *Semin. Radiat. Oncol.* **1998**, *8*, 176–182.

Published on Web 08/12/2009

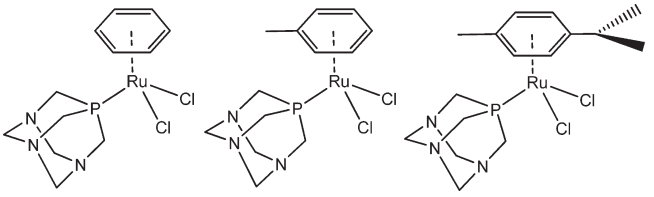

Figure 1. Examples of [Ru(η^6-arene)(pta)Cl_2] compounds: (left) RAPTA-B, arene = benzene; (center) RAPTA-T, arene = toluene; and (right) RAPTA-C, arene = *p*-cymene.

RAPTA-C induces significant unwinding of supercoiled DNA at pH values below 7 without exerting an effect on DNA at physiological pH.[9] Indeed, another recent study has shown that binding of RAPTA-C to potential biomolecular targets is an order of magnitude higher at pH 6 compared to pH 7.2.[10] Theoretical and experimental studies indicate that the active and nonactive species of RAPTA-type complexes are, respectively, the aqua and hydroxo forms derived from hydrolysis of one of the chloride ligands. So far it has not been possible to observe the deprotonation reaction by ^{1}H NMR spectroscopy, as a significant broadening of the diagnostic arene signals occurs at higher pH; however, DFT calculations estimate the pK_a to be around pH 9 for RAPTA-B, implying that the dominant species at physiological pH is the aqua complex, which shows greater ligand labiality, and hence reactivity.[11]

With the aim of exploiting the pH difference between a tumor cell and healthy cell environment, DFT calculations were carried out to design a complex for which the major species in a healthy cell would be the less reactive hydroxo compound, with the more active aqua compound dominating in the lower pH environment of a tumor. Accordingly, strongly electron-withdrawing groups attached to the arene ring were shown to modulate the equilibrium between the hydroxo- and aqua-containing complexes. In this respect fluorine-substituted aromatic groups provide an ideal means of lowering the pK_a without greatly modifying the steric profile or hydrophilic properties of RAPTA-type complexes. However, such electron-poor arenes are comparatively weak ligands, and few examples of ruthenium(II)-fluoroarene compounds have been reported, the majority being sandwich complexes of general formula [Ru(η^5-C_5Me_5)(η^6-fluoroarene)]$^+$, for which a general synthetic procedure has been developed.[12] Therefore, we have investigated the synthesis of several RAPTA complexes with fluoroarene ligands, viz., [Ru(η^6-fluoroarene)(pta)Cl_2], and herein describe these compounds and discuss the effects of the η^6-bound fluorous arene ligand on stability, hydrolysis, pK_a, and cell proliferation.

Results and Discussion

The new RAPTA compounds with fluoroarene ligands shown in Figure 2 were prepared following a multistep synthesis involving reduction to a Ru(0) species and subsequent oxidation to regenerate the Ru(II)-fluoroarene species. This is in contrast to the previously reported synthesis of RAPTA complexes, which involves two steps: reduction of hydrated $RuCl_3$ with the appropriate hexacyclic diene to give a chloro-bridged arene dimer,[13] followed by reaction of the dimer with 2 equiv of the pta ligand. The diene is usually obtained through Birch reduction of the corresponding arene; however, in the case of halogenated arenes, Birch reduction is dangerous, possibly resulting in the formation of the highly reactive and potentially explosive arynes. An alternative procedure involves thermally induced arene exchange, which has been used to generate η^6-C_6Me_6- or η^6-$C_6H_3(^iPr)_3$-substituted chloro-ruthenium(II) dimers from the corresponding *p*-cymene species at 180 °C.[13c] However, our attempts to substitute *p*-cymene with the electron-withdrawing $CF_3C_6H_5$ arene by thermal or photochemical methods were unsuccessful, as similarly reported by the research group of Bennett, who failed to displace η^6-benzene or *p*-cymene with $C_6H_5CF_3$ from Ru(η^6-arene)Cl_2{P(*n*Bu)$_3$} by irradiation with ultraviolet light.[13c] Consequently, a seldom used route (Scheme 1) was used to prepare the dimeric precursors.

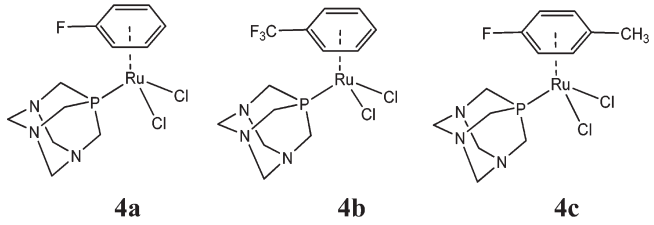

4a **4b** **4c**

Figure 2. Structures of new fluoroarene-substituted RAPTA compounds **4a**−**4c**.

The synthesis of **4a**−**4c** commences with [Ru(acac)$_2$(η^4-cod)] (**1**), first reported by Wilkinson, for which an improved synthesis was described by Powell et al. and employed for this work. Compound **1** is converted to the reactive ruthenium(0) species [Ru(η^6-napthalene)(η^4-cod)] using a modified but established procedure reported by the groups of Bennett and Vitulli.[14] This compound readily undergoes facile exchange of the 10-electron naphthalene ligand with the appropriate fluoroarene, in the presence of a small amount of acetonitrile, to give [Ru(η^6-fluoroarene)(η^4-cod)] (fluoroarene = C_6H_5F **2a**, $C_6H_5CF_3$ **2b**, 1,4-$C_6H_4CH_3F$ **2c**, and 1,4-$C_6H_4F_2$ **2d**).[15] In all cases, chromatographic separation was required using slightly basic alumina as the stationary phase and eluting with pentane. Compound **2a** and *meta* analogues of **2c** and **2d**, i.e., [Ru(η^6-1,3-$C_6H_4CH_3F$)(η^4-cod)] and [Ru(η^6-1,3-$C_6H_4F_2$)(η^4-cod)], are known compounds.[15] While the mono- and difluoro complexes were successfully prepared by the described method, 1,3,5-trifluorobenzene proved to be too weakly coordinating to displace the naphthalene ligand, with attempts involving low-pressure hydrogenation of [Ru(η^4-cot)(η^4-cod)] (cot = cyclooctatetraene) also proving unsuccessful.[16]

(9) Allardyce, C. S.; Dyson, P. J.; Ellis, D. J.; Heath, S. L. *Chem. Commun.* **2001**, 1396–1397.
(10) Groessl, M.; Hartinger, C. G.; Dyson, P. J.; Keppler, B. K. *J. Inorg. Biochem.* **2008**, *102*, 1060–1065.
(11) Gossens, C.; Dorcier, A.; Dyson, P. J.; Rothlisberger, U. *Organometallics* **2007**, *26*, 3969–3975.
(12) (a) Koelle, U.; Hoernig, A.; Englert, U. *Organometallics* **1994**, *13*, 4064–4066. (b) Fang, X.; Watkin, J. G.; Scott, B. L.; John, K. D.; Kabas, G. J. *Organometallics* **2002**, *21*, 2336–2339. (c) Hayashida, T.; Nagashima, H. *Organometallics* **2002**, *21*, 3884–3888.
(13) (a) Winkhaus, G.; Singer, H. *J. Organomet. Chem.* **1967**, *7*, 487–491. (b) Zelonka, R. A.; Baird, M. C. *Can. J. Chem.* **1972**, *50*, 3063–3072. (c) Bennett, M. A.; Smith, A. K. *Dalton Trans.* **1974**, 233–241.
(14) Bennett, M. A.; Neuman, H.; Thomas, M.; Wang, X.; Pertici, P.; Salvadori, P.; Vitulli, G. *Organometallics* **1991**, *10*, 3237–3245.
(15) Bodes, G. F.; Heinemann, W.; Jobi, G.; Klodwig, J.; Neumann, S.; Zenneck, U. *Eur. J. Inorg. Chem.* **2003**, 281–292.
(16) Pertici, P.; Vitulli, G.; Lazzaroni, R.; Salvadori, P.; Barili, P. L. *Dalton Trans.* **1982**, 1019–1022

Scheme 1. Synthetic Routes Employed for 4a−4d[a]

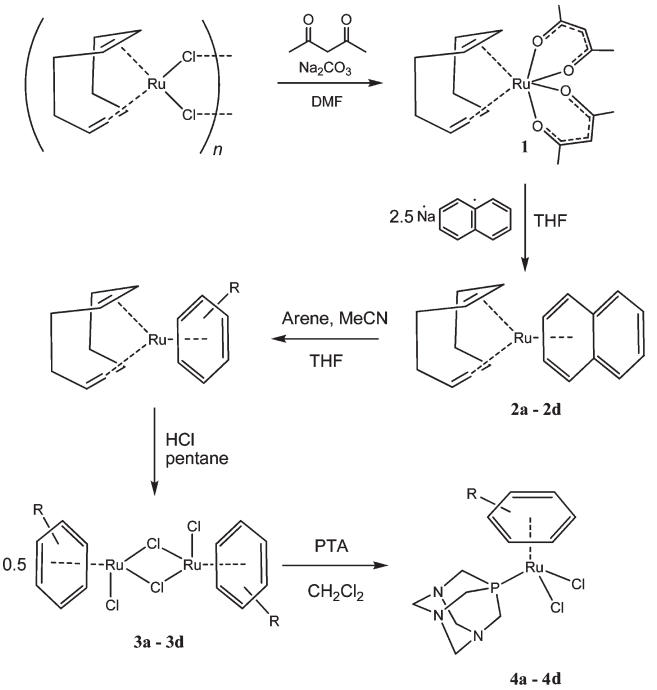

[a] R represents a fluoroarene, i.e., C_6H_5F **1a**−**4a**, $C_6H_5CF_3$ **1b**−**4b**, 1,4-$CH_3C_6H_4F$ **1c**−**4c**, and 1,4-$C_6H_4F_2$ **1d**−**4d**.

The [Ru(η^6-fluoroarene)(η^4-cod)] complexes, **2a**−**2d**, are oxygen sensitive both in solution and in the solid state, but readily crystallize by evaporation of a saturated pentane solution. ^{1}H and ^{13}C NMR spectra each show two signals characteristic of the cyclooctadiene ligand in addition to the peaks corresponding to the η^6-bonded fluoroarene ligand. The conversion of **2a**−**2d** into chloride-bridged dimers (**3a**−**3d**) follows a modified literature method involving the addition of 2 equiv of gaseous HCl in pentane, oxidizing the Ru(0) to Ru(II) with concomitant reduction of the cod ligand to cyclooctane. The extremely poor solubility of the chloro-bridged dimeric species excluded their complete spectroscopic characterization. Nevertheless, the corresponding [Ru(η^6-fluoroarene)(pta)Cl_2] complexes are readily prepared in good yield from the dimers by addition of 2 equiv of pta in dichloromethane. Complexes **4a**−**4c** are stable to air, and **4c** is soluble in water and polar organic solvents, while **4a** and **4b** are only sparingly soluble. Compound **4d** could not be prepared in pure form and therefore was not studied further.

X-ray Diffraction Studies. Single-crystal X-ray diffraction was used to characterize **4a** and **4c** and a number of the intermediate compounds involved in their preparation, namely, **1** and **2a**−**d**. No single crystals of the dimers were obtained due to their insolubility in organic solvents. In contrast, all of the [Ru(η^6-fluoroarene)(η^4-cod)] complexes, **2a**−**d**, readily formed large and highly crystalline yellow or orange needles and blocks. The molecular structure of the parent compound of the series with the naphthalene ligand, [Ru(acac)$_2$(η^4-cod)] (**1**), has been previously described.[17] However, only powder X-ray diffraction data of **1** are available,[18] despite being first reported in 1959.[19] Using slightly different crystallization procedures from those described previously, we obtained single crystals that gave different cell parameters and the space group $P2_1/n$, instead of $P2_1/c$, in contrast with the powder X-ray data. The structure of **1** is shown in Figure 3, with selected bond lengths and angles provided in the caption. The complex is characterized by a six-coordinate, pseudo-octahedral Ru geometry. All of the Ru−O bonds are equivalent in length within experimental error, as are the two C═C bonds. A search of the CSD[20] reveals that only seven previously reported complexes are known that feature two acteylacetone groups bound to Ru, along with a ligand (or ligands) with two C═C bonds. In the case of **1**, the C═C bonds are orientated nearly parallel with one another, as indicated by the C═C···C═C torsion angle of 7.65(2)°. This contrasts with acyclic species featuring two ethene groups, i.e., Ru(acac)$_2$-(η^2-H_2C═CH_2)$_2$, where the equivalent angle is 76.4(1)°. In **1** both the internal O−Ru−O bond angles and the external O(2)−Ru−O(3) angles are equivalent, these parameters being similar to those observed in other Ru-acac complexes with coordinated unsaturated hydrocarbon co-ligands.

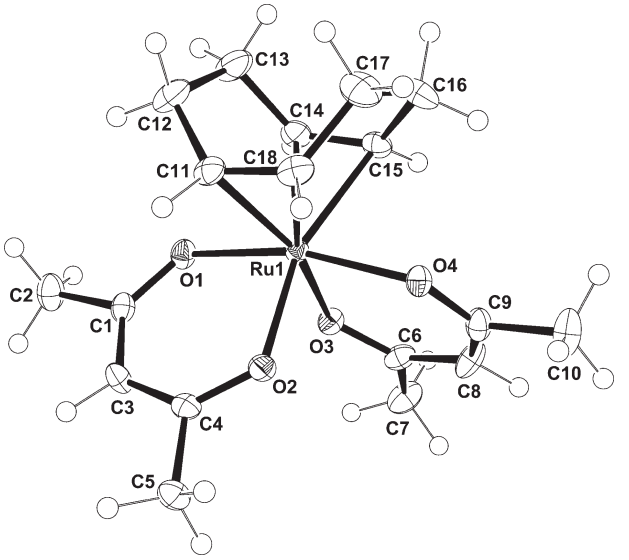

Figure 3. ORTEP plot of **1** with non-hydrogen atoms represented by thermal parameters with 50% probably ellipsoids. Selected bond lengths (Å) and angles (deg): Ru(1)−O(1) 2.066(2), Ru(1)−O(2) 2.064(2), Ru(1)−O(3) 2.058(2), Ru(1)−O(4) 2.074(2), Ru(1)−C(11) 2.177(2), Ru(1)−C(14) 2.167(2), Ru(1)−C(15) 2.169(2), Ru(1)−C(18) 2.172(2 O(1)−Ru(1)−O(2) 89.84(6), O(3)−Ru(1)−O(4) 89.76(6), O(2)−Ru(1)−O(3) 89.34(6), Ru(1)−O(1)−C(1) 124.95(15), Ru(1)−O(2)−C(4) 125.34(15), Ru(1)−O(3)−C(6) 126.15(15), Ru(1)−O(4)−C(9) 124.52(15), C(11)−Ru(1)−C(18) 36.87(9), C(14)−Ru(1)−C(15) 36.73(9), C(11)−Ru(1)−C(14) 81.22(9), C(14)−Ru(1)−C(15) 36.73(9).

The structures of **2a**−**2d** are shown in Figure 4, and a comparison of selected bond parameters is provided in Table 1 along with the naphthalene-based precursor and the benzene analogue reported previously.[21] Complex **2b** represents the first crystallographically characterized structure to feature a $C_6H_5CF_3$ ligand η^6-bound to a Ru center. The structure of **2a** contains two crystallographically

(17) Crocker, M.; Green, M.; Howard, J. A. K.; Norman, N. C.; Thomas, D. M. *Dalton Trans.* **1990**, 2299–2301.
(18) (a) Potvin, C.; Manoli, J. M.; Dereigne, A.; Pannetier, G. *J. Less Common Met.* **1971**, *24*, 333–334. (b) Potvin, C.; Pannetier, G. *J. Less Common Met.* **1970**, *22*, 91–98.
(19) Bennett, M. A.; Wilkinson, G. *Chem. Ind.* **1959**, 1519.
(20) Allen, F. H. *Acta Crystallogr.* **2002**, *B58*, 380–388.
(21) Schmid, M.; Ziegler, M. L. *Chem. Ber.* **1976**, *109*, 132–138.

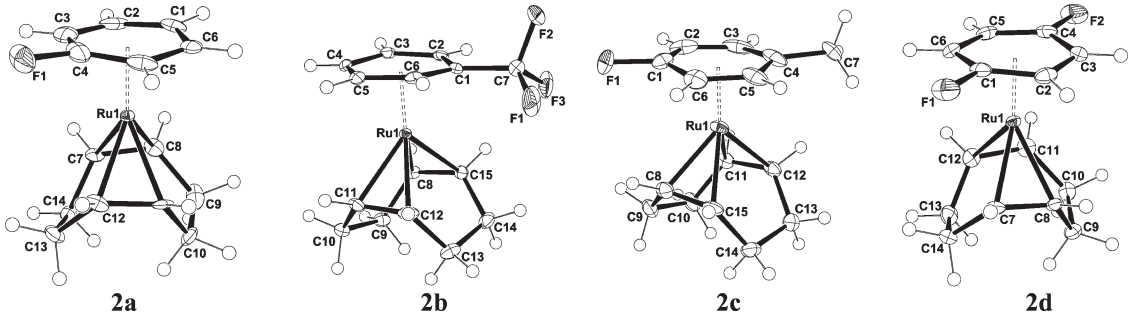

Figure 4. ORTEP plots of **2a**−**2d** with non-hydrogen atoms represented by thermal parameters with 50% probably ellipsoids. The disorder of the F atom (**2a**) and CH_3 group and F atoms (**2c**) has been omitted for clarity. Selected bond lengths and angles are given in Table 1.

Table 1. Comparison of Selected Bond Lengths (Å) and Angles (deg) of 2a−2d and Analogues with Naphthalene ($C_{10}H_8$) and Benzene (C_6H_6)

	2a Ar = C_6H_5F [a,b]	**2b** Ar = $C_6H_5CF_3$	**2c** Ar = $C_6H_4(F)CH_3$	**2d** Ar = $C_6H_4F_2$	Ar = $C_{10}H_8$	Ar = C_6H_6
centroid(Ar)−Ru	1.760(2) 1.752(2)	1.751(1)	1.749(2)	1.746(1)	1.780(1)	1.750[c]
Ru−C(=C)	2.156(5) 2.138(5) 2.152(5) 2.140(5) 2.141(5) 2.151(5) 2.157(5) 2.169(5)	2.169(2) 2.161(2) 2.151(1) 2.153(2)	2.082(4) 2.147(3) 2.167(3) 2.116(4)	2.159(3) 2.140(3) 2.157(2) 2.165(2)	2.126(3) 2.131(3) 2.141(3) 2.142(3)	2.134(5) 2.133(5) 2.132(5) 2.148(5)
average	2.147(10) 2.155(10)	2.159(4)	2.128(7)	2.155(6)	2.135(6)	2.135(10)
range	0.018(7) 0.028(7)	0.018	0.085	0.019	0.016	0.016
C=C	1.431(7) 1.431(7)	1.419(3) 1.431(3)	1.457(5) 1.471(4)	1.428(4) 1.432(4)	1.418(4) 1.414(4)	1.403(11) 1.423(8)
centroid(Ar)−Ru−*mp*(C=C)[d]	136.31(14) 137.80(14)	136.90(5) 137.80(5)	136.83(9) 138.65(9)	137.09(7) 137.08(7)	136.58(8) 137.03(9)	137.68[c] 136.83[c]
mp(C=C)−Ru−*mp*(C=C)	85.89(14)	85.29(6)	84.52(10)	85.84(8)	86.38(9)	85.49[c]
(HC)H···C(=C)	2.732 2.825	2.679 2.825	2.791 2.792	n/a	2.852	n/a

[a] Structure contains two crystallographically independent molecules in the unit cell. [b] The arene component of the molecule is disordered over two positions. [c] No atomic position esd's provided in the cif file to calculate the esd of the centroid or midpoint of the C=C bonds. [d] The abbreviation *mp* refers to midpoint or bisection point of the two C=C bonds of the cod group.

independent molecules in the unit cell, each molecule having a slightly different geometry, with the primary difference corresponding to the amount of $(H_2)C-C(H_2)$ single-bond twisting within the cod ligand. Furthermore, **2a** and **2c** feature positional disorder of the F atom over two sites, which was resolved using a standard method (see Experimental Section).

The distance between the Ru atom and the centroid of the fluoroarene ligands is considerably shorter than in the naphthalene complex, which is correlated with the highly labile nature of this particular arene ligand. The average bond distances between the Ru center and olefin bond are equal in all the systems; however, in complex **2c** the distance is significantly different, i.e., by 0.085 Å. For **2a**−**2d** the two C=C bonds of the cod are not coplanar and are twisted in opposing directions. The greatest amount of twisting, as measured at the C=C bisection point, is observed in complex **2d** [9.2(2)°]. Such a distortion is probably due to a combination of electronic effects from the two electron-withdrawing fluorine atoms, which also exert a slightly greater steric interaction on the cod group. As a final point, in contrast to the benzene and naphthalene complexes, and as expected with the introduction of F atoms, a substantial number of hydrogen-bonding interactions are present, but will not be discussed here.

The structures of **4a** and **4c** are shown in Figure 5. Both **4a** and **4c** comprise a Ru center with a distorted piano-stool geometry. The rotation of the arene in **4c** is such that the bulkier methyl group does not eclipse the Ru−Cl or Ru−P bonds. However, in **4c** partial eclipsing of the (Ar)C−F bond with a Ru−Cl bond is observed. Table 2 lists the relevant metric parameters of **4a** and **4c** with a comparison of the previously reported *p*-cymene-containing structure, RAPTA-C.[22] In general, bond parameters of **4c** and RAPTA-C are very similar, with **4a** being somewhat different. The internal structural parameters of the pta ligand are identical for all of the complexes.

Structure **4c** differs from **4a** and RAPTA-C in that no solvate molecules are found in the unit cell. Instead, a tight packing of the molecules is observed with short intermolecular hydrogen-bonding interactions. An arene−arene π-stacking interaction is observed, with the shortest interarene

(22) Allardyce, C. S.; Dyson, P. J.; Ellis, D. J.; Heath, S. L. *Chem. Commun.* **2001**, 1396–1397.

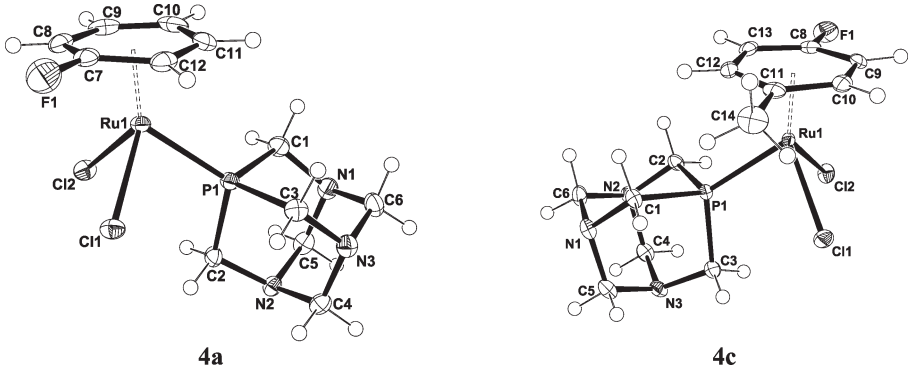

Figure 5. ORTEP plots of **4a** and **4c** with non-hydrogen atoms represented by thermal parameters with 50% probably ellipsoids. Selected bond lengths and angles are given in Table 2.

Table 2. Selected Bond Lengths (Å) and Angles (deg) of 4a, 4c, and RAPTA-C

parameter	4a	4c	RAPTA-C[a]
Ru−Ar(centroid)	1.725(1)	1.705(1)	1.692(4)
			1.701(4)
Ru−Cl	2.434(1)	2.410(1)	2.412(3)
	2.431(1)	2.411(1)	2.429(3)
			2.425(3)
			2.425(3)
Ru−P	2.279(1)	2.297(1)	2.296(2)
			2.298(3)
P−C(N)	1.843(2)	1.839(2)	1.840(11)
	1.839(3)	1.845(2)	1.837(10)
	1.840(3)	1.846(2)	1.855(8)
			1.827(10)
			1.834(11)
			1.831(10)
N−C(N)	1.477(3)	1.477(3)	1.470(12)
	1.481(3)	1.472(3)	1.489(12)
	1.503(3)	1.475(3)	1.448(10)
			1.474(12)
			1.465(13)
			1.471(13)
Cl−Ru−Cl	87.78(2)	87.88(2)	87.25(9)
			88.97(9)
Cl−Ru−P	84.62(2)	86.19(2)	87.09(10)
	87.86(2)	82.61(2)	83.42(9)
			85.29(10)
			82.79(9)
centroid(Ar)−Ru−P	131.20(4)	129.68(3)	129.60(15)
			120.76(15)
centroid(Ar)−Ru−Cl	123.63(4)	127.09(3)	126.85(19)
	127.50(4)	128.29(3)	127.86(17)
			127.78(18)
			127.23(16)
Ru−P−C	116.92(8)	115.44(7)	117.3(3)
	119.37(8)	119.98(7)	119.9(3)
	120.49(8)	120.82(7)	119.9(3)
			118.0(3)
			119.7(3)
			119.1(4)
C−P−C	97.82(12)	98.58(9)	98.4(4)
	98.52(12)	98.31(9)	98.6(5)
	99.31(11)	99.45(10)	98.2(4)
			99.9(5)
			98.0(4)
			97.7(5)

[a] Structure contains two crystallographically independent molecules within the unit cell. Taken from ref 23.

distance being 3.283(3) Å. A strong intermolecular hydrogen bond (2.65 Å) between the methyl group and F atom probably assists in enforcing this stacking arrangement. In **4a** a similar arene−arene π-stacking arrangement is observed, except the slippage is greater, and the shortest interarene distance is 3.351(4) Å. Furthermore, the unit cell is extremely large and a high amount of void space is present. Within this space is an array of interconnected disordered water molecules that form a number of intermolecular hydrogen bonds within the complex, specifically at the ring fluorine group, chlorine, and the hydrogen atoms of the pta ligand. Interestingly, the nitrogen centers of the pta are not involved in hydrogen bonding with the water solvates, which is generally thought to be responsible for the high degree of water solubility associated with the pta ligand.[23]

Characterization of 4a−4c in Aqueous Solution. The behavior of **4a−4c** in aqueous solution was carefully monitored by ^{1}H and ^{31}P NMR spectroscopy. RAPTA-type complexes have previously been shown to undergo rapid hydrolysis in water through loss of a chloride ligand (eq 1), to reach an equilibrium between the dichloro and monochloro complexes.[7] The hydrolysis product is observed in the ^{31}P NMR spectrum by a second peak, ca. 2 ppm downfield of the starting compound, and the process is reversed through the addition of sodium chloride.

In contrast to the benzene- and alkyl substituted arene RAPTA compounds, hydrolysis of **4a−4c** is not rapid, and a new peak corresponding to the hydrolysis species is visible in the ^{31}P NMR spectrum only after approximately 30 min in solution, with **4a** and **4c** reaching equilibrium after 2 h and **4b** only after ca. 1 day. When the concentration of Cl^- is increased to 100 mM, the ^{31}P NMR signal for the hydrolysis product is not observed following 3 days in solution; however, in the case of **4b**, and to a lesser extent **4c**, a new species appears that exhibits a peak at ca. 1 ppm from the original peak. The presence of free arene in the ^{1}H NMR spectra suggests that this species results from the loss of the arene ligand. While it was not possible to obtain a crystal structure for **4b**, it is not unreasonable to expect the Ru−arene bond to be relatively weak given the electron-withdrawing nature of the arene ligand. Indeed the Ru−arene bond length of the precursor complex **2b** is considerably elongated; see Table 1.

Uniquely in the case of **4b**, the rate of hydrolysis was found to increase progressively on the addition of acid with a 5-fold increase in rate observed on going from pH 5.7 (unbuffered solution) to 4.7 (Table 3, Figure 6). This rate increase may be due to more extensive hydrogen bonding between the chloride ligands and protons in solution, thereby activating the Ru−Cl bond. Consequently, it is conceivable that the

(23) Phillips, A. D.; Gonsalvi, L.; Romerosa, A.; Vizza, F.; Peruzzini, M. *Coord. Chem. Rev.* **2004**, *248*, 955.

formation of the labile aqua complex would occur more quickly in a cancerous cell than a healthy cell, also potentially contributing to drug selectivity.

^{31}P NMR-based titrations were used to determine the pK_a values for the *N*-protonation of the pta ligand in **4a**−**4c** (pK_a 1, eq 2, Table 4). It was not possible to observe deprotonation of the water ligand by NMR (pK_a 2, eq 3). The pK_a 1 values were unchanged within experimental error when the measurements were repeated with a Cl^- concentration of 100 mM.

$$[Ru(\eta^6\text{-arene})(pta)Cl_2] \underset{+Cl^- -H_2O}{\overset{+H_2O,\,Cl^-}{\rightleftharpoons}} [Ru(\eta^6\text{-arene})(pta)Cl(H_2O)]^+ \quad (1)$$

$$[Ru(\eta^6\text{-arene})(pta)Cl_2] \underset{-H^+}{\overset{H^+}{\rightleftharpoons}} [Ru(\eta^6\text{-arene})(pta\text{-}H)Cl_2]^+ \quad (2)$$

$$[Ru(\eta^6\text{-arene})(pta)Cl(OH)] \underset{-H^+}{\overset{H^+}{\rightleftharpoons}} [Ru(\eta^6\text{-arene})(pta)Cl(H_2O)]^+ \quad (3)$$

In general, the calculations underestimate the experimental pKa 1 values by 0.12−1.04 units. Most of the alkyl and fluorinated substituted systems have similar calculated and experimental values, ranging from 1.9−2.9 and 2.12−3.31, respectively. However, the calculated pK_a values of the $C_6H_5CF_3$- and 1,4-FC_6H_4Me-containing complexes **4b** and **4c** are significantly reduced (2.0) compared to the other calculated values. In particular **4b** is nearer to the experimentally observed value with a difference of 0.07, accounting for the error factor associated with the experimental value. With the exception of compound **4c** and RAPTA-C, the theoretical and experimental values for the first pK_a follow the same trend, namely, decreasing in the order RAPTA-T > RAPTA-B > RAPTA-F (**4a**) > RAPTA-CF_3 (**4b**). For RAPTA-C and **4c**, featuring sterically more demanding arene ligands, the differences between calculated and experimental values are larger.

Table 3. k_{obs} for the Hydrolysis of 4b

solution pH	$k_{obs}(s^{-1})$
5.7	$7.05 \times 10^{-5} \pm 3.65 \times 10^{-6}$
4.7	$3.70 \times 10^{-4} \pm 7.51 \times 10^{-5}$

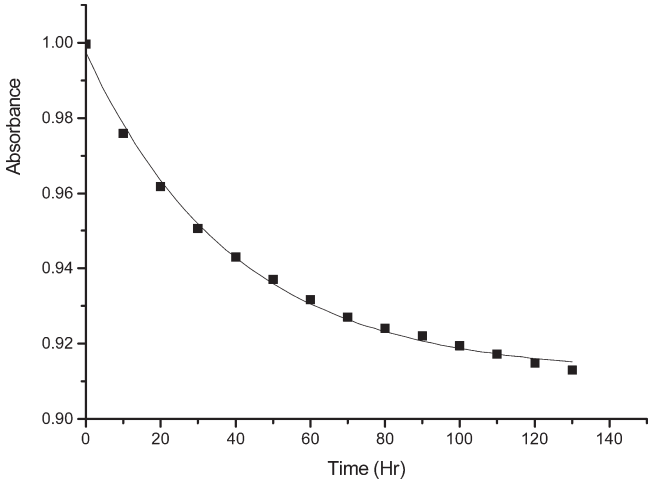

Figure 6. Decay of absorbance at 355 nm for **4b** (pH 5.7 in unbuffered solution). Data fitted to Abs = $A_0 \exp(-k_{obs}t) + A_1$.

Regarding the protonation of the ruthenium-bound OH ligand (pK_a 2), calculations predict remarkably lower values for the doubly and triply fluorinated compounds (5.1−6.0) than for the nonfluorinated and singly fluorinated compounds (8.2−9.2). The pK_a 2 values follow the trend RAPTA-B > **4c** > RAPTA-C > **4a** > RAPTA-T ≫ RAPTA-F2 > **4b** > RAPTA-F3, decreasing with increasing number of electron-withdrawing substituents on to η^6-arene ligand.

With the exception of **4c**, proton affinities (PA) and gas phase basicities (GB) of the OH group of the fluoroarene compounds are all lower than the other compounds (GB 230−234 vs 237−240 kcal mol^{-1}, respectively) and indicate that the decrease in pK_a 2 is mainly due to electronic effects rather than solvation effects. Comparing the values of PA and GB for the pta and the OH groups, the calculations predict an absolute decrease of the negative electrostatic potential (ESP) induced by the F-substitution for the OH group, compared to the more distant N atoms of the pta ligand.

The pK_a 2 of **4a** and **4c** is greater than 7.2, indicating that similar to known RAPTA compounds, the labile aqua complex would be the dominant species at cellular pH. In contrast, **4b**, RAPTA-F2, and RAPTA-F3 have calculated pK_a 2 values below 6.8, indicating that the hydroxyl form would be expected to dominate at cellular pH and the more reactive aqua form at the reduced pH of cancer tissue, potentially providing a greater selectivity in that they should be more reactive in the reduced pH environment of cancer tissue and less reactive in healthy tissue, where the pH is ca. 7.2.

Cytotoxicity Assays. The cyctotoxicity of **4a**−**4c** was evaluated in the A2780 human ovarian cancer cell line using the colormetric MTT assay (Table 6). Complex **4a** is less active than the benchmark compound, RAPTA-C, also included as a control. In contrast, **4b** and **4c** are significantly more cytotoxic than RAPTA-C, and it is noteworthy that the most active compound, i.e., **4b**, corresponds to the one predicted to have the most relevant pK_a 2 value from the computational study. It is also possible that the more labile arene ligand in **4b** and **4c**, compared to other RAPTA

Table 4. Calculated and Experimentally Determined pK_a 1 Values with the Corresponding Proton Affinities (PA), Gas Phase Basicities (GB), and Dipole Moments (μ)

complex	arene	pK_a 1 (expt)	pK_a 1 (calc)	ΔpK_a 1 (pK$_a$(expt) - pK$_a$(calc))	PA (kcal mol^{-1})	GB (kcal mol^{-1})	μ (Db)
RAPTA-C	1,4-^{i}PrC_6H_4Me	3.13 ± 0.02[a]	2.1[b]	1.03	222.1[b]	219.3[b]	7.49[b]
RAPTA-B	C_6H_6	3.23 ± 0.06[a]	2.8[b]	0.43	228.1	220.5	7.41
RAPTA-T	$C_6H_5CH_3$	3.31 ± 0.03[a]	2.9	0.41	228.9	221.3	7.21
RAPTA-F (**4a**)	C_6H_5F	3.13 ± 0.04	2.5 (2.9)	0.63	226.5	219.2	7.96
RAPTA-CF3 (**4b**)	$C_6H_5CF_3$	2.12 ± 0.05	2.0 (2.6)	0.12	224.3	216.8	8.91
RAPTA-FT (**4c**)	1,4-$FC_6H_4CH_3$	3.04 ± 0.04	2.0 (2.2)	1.04	227.5	219.8	7.78
RAPTA-F2	1,4-$C_6H_4F_2$	–	2.30	–	225.7	218.2	7.04
RAPTA-F3	1,3,5-$C_6H_3F_3$	–	1.9[b]	–	224.4[b]	216.9[b]	6.65[b]

[a] Data taken from ref 5. [b] Data taken from ref 8.

Table 5. Calculated pK_a 2 Values with the Corresponding Proton Affinities (PA) and Gas Phase Basicities (GB)[a]

complex	arene	pK_a 2 (calc)	PA (kcal mol^{-1})	GB (kcal mol^{-1})
RAPTA-C	1,4-^{i}PrC$_6$H$_4$Me	8.7	246.6	239.4
RAPTA-B	C$_6$H$_6$	9.2[b]	243.9[b]	240.5[b]
RAPTA-T	C$_6$H$_5$CH$_3$	8.2	244.6	237.8
RAPTA-F (**4a**)	C$_6$H$_5$F	8.3 (8.1)	242.3	234.8
RAPTA-CF3 (**4b**)	C$_6$H$_5$CF$_3$	5.5 (6.1)	242.1	234.1
RAPTA-FT (**4c**)	1,4-FC$_6$H$_4$CH$_3$	8.9 (8.2)	245.7	238.5
RAPTA-F2	1,4-C$_6$H$_4$F$_2$	6.0	238.2	231.3
RAPTA-F3	1,3,5-C$_6$H$_3$F$_3$	5.1[b]	238.1[b]	230.9[b]

[a] All values were calculated for the conformers with highest solvation energies. The pK_a values for the conformer that is most stable in the gas phase are given in parentheses. [b] Data taken from ref 8. [c] Data taken from ref 8.

Table 6. IC_{50} Values of 4a−4c and RAPTA-C in A2780 Cells

complex	IC_{50} (μM)
RAPTA-C	353
RAPTA-F (**4a**)	507
RAPTA-CF3 (**4b**)	38
RAPTA-FT (**4c**)	78

compounds, contributes to their greater cytotoxicity. Indeed, it has been shown that, following binding to a model oligonucleotide, RAPTA derivatives lose the arene ligand,[24] and such a process is likely to result in increased distortions to the oligonucleotide structure due to increased coordination demands of the complex. It should be noted that while RAPTA-C is scarcely toxic, it is highly effective *in vivo*, displaying good activity against both metastatic[7] and primary tumors,[25] albeit at high doses. Thus while the greater cytotoxicity of **4b** and **4c** may lead to activity against different tumors, they are likely to be applicable at much lower doses than RAPTA-C, which is very interesting from a pharmacological point of view.

Conclusions

Rationally designed organometallic compounds are attracting increasing attention as potential anticancer drugs.[26] In this context organoruthenium(II) compounds show much promise,[27] following early studies showing that compounds of this type could react with biologically relevant targets.[28] In this paper a series of RAPTA-type complexes with fluoro-substituted η^6-arene ligands have been prepared and characterized using several techniques. In particular the hydrolysis behavior has been compared with other previously reported RAPTA compounds. pK_a values for the protonation of the pta ligand were predicted by DFT with reasonable accuracy for complexes containing mono F-substituted arene ligands; however, the method was less effective for di-F-substituted arenes and the trifluoromethyl derivative. The electron-withdrawing fluoroarene ligands modulate the pK_a's of the complexes, strongly influencing their behavior in solution and leading to comparatively low IC_{50} values. Moreover, the pH-dependent hydrolysis of **4b** may prove to be an effective "built-in" mechanism for selectively targeting cancerous tissue while sparing healthy tissue due to their intrinsic differences in pH. It is not unreasonable to assume that **4b** would hydrolyze only in the reduced pH environment of a tumor, thus becoming active and able to induce cell death. In healthy tissue **4b** should be considerably less labile and therefore less toxic.

Experimental Section

$[Ru(\eta^4\text{-}C_8H_{12})Cl_2]_n$, $[Ru(\eta^4\text{-}C_8H_{12})(\eta^6\text{-napthalene})]$, and pta were prepared according to literature methods.[29,14,30] Compounds were prepared under an inert atmosphere using dried and degassed solvents. ^{1}H, ^{13}C, and ^{31}P NMR spectra were recorded at 400 MHz on a Bruker Avance DPX spectrometer at room temperature. ^{19}F NMR spectra were recorded at 200 MHz on a Bruker Avance DPX spectrometer at room temperature. ESI-MS of the complexes were obtained on a Thermo Finnigan LCQ Deca XP Plus quadrupole ion trap instrument set in positive mode (solvent: methanol; flow rate: 5 μL/min; spray voltage: 5 kV; capillary temperature: 100 °C; capillary voltage: 20 V), as described previously.[31]

Synthesis of $[Ru(\eta^4\text{-}C_8H_{12})(acac)_2]$, 1. A modified synthesis of the one reported by Powell was used.[32] To a two-neck flask with reflux condenser and gas-inlet was added $[Ru(\eta^4\text{-}C_8H_{12})Cl_2]_n$ (2.72 g, 10 mmol) and anhydrous Na_2CO_3 (10 g, Fluka). The flask and its contents were evacuated and flushed with N_2. A solution of 2,4-pentanedione (2.925 g, Aldrich, vacuum distilled) in DMF (50 mL, Acros, degassed and dried over 4 Å molecular sieves) was added to the reaction flask via cannula. The resulting orange solution was heated at 150 °C for 30 min, and the solution was filtered in air while hot. Additional DMF (15 mL) was added to wash the flask and frit. Doubly distilled water (135 mL) was added to the filtrate, over a period of 1 h, causing the precipitation of an orange-yellow solid. The product

(24) Scolaro, C.; Geldbach, T. J.; Rochat, S.; Dorcier, A.; Gossens, C.; Bergamo, A.; Cocchietto, M.; Tavernelli, I.; Sava, G.; Rothlisberger, U.; Dyson, P. J. *Organometallics* **2006**, *25*, 756–765.
(25) Chatterjee, S.; Kundu, S.; Bhattacharyya, A.; Hartinger, C. G.; Dyson, P. J. *J. Biol. Inorg. Chem.* **2008**, *13*, 1149–1155.
(26) For example see: (a) Nguyen, A.; Top, S.; Pigeon, P.; Vessieres, A.; Hillard, E. A.; Plamont, M.; Huche, M.; Rigamonti, C.; Jaouen, G. *Chem. Eur. J.* **2009**, *15*, 684–696. (b) Top, S.; Thibaudeau, C.; Vessieres, A.; Brule, E.; Le Bideau, F.; Joerger, J.; Plamont, M.; Samreth, S.; Edgar, A.; Marrot, J.; Herson, P.; Jaouen, G. *Organometallics* **2009**, *28* (5), 1414–1424. (c) Strohfeldt, K.; Tacke, M. *Chem. Soc. Rev.* **2008**, *37*, 1174–1187. (d) Hogan, M.; Claffey, J.; Pampillon, C.; Tacke, M. *Med. Chem.* **2008**, *4*, 91–99. (e) Kirin, S. I.; Ott, I.; Gust, R.; Mier, W.; Weyhermueller, T.; Metzler-Nolte, N. *Angew. Chem.* **2008**, *47*, 955–959. (f) Gross, A.; Metzler-Nolte, N. *J. Organomet. Chem.* **2009**, *694*, 1185–1188. (g) Zobi, F.; Blacque, O.; Sigel, R. K. O.; Alberto, R. *Inorg. Chem.* **2007**, *46*, 10458–10460. (h) Xavier, C.; Giannini, C.; Dall'Angelo, S.; Gano, L.; Maiorana, S.; Alberto, R.; Santos, I. *J. Biol. Inorg. Chem.* **2008**, *13*, 1335–1344. (i) Hartinger, C. G.; Dyson, P. J. *Chem. Soc. Rev.* **2009**, *38*, 391–401.
(27) (a) Romerosa, A.; Saoud, M.; Campos-Malpartida, T.; Lidrissi, C.; Serrano-Ruiz, M.; Peruzzini, M.; Garrido, J. A.; Garcia-Maroto, F. *Eur. J. Inorg. Chem.* **2007**, *18*, 2803–2812. (b) Schmid, W. F.; John, R. O.; Arion, V. B.; Jakupec, M. A.; Keppler, B. K. *Organometallics* **2007**, *26*, 6643–6652. (c) Habtemariam, A.; Melchart, M.; Fernandez, R.; Parsons, S.; Oswald, I. D. H.; Parkin, A.; Fabbiani, F. P. A.; Davidson, J. E.; Dawson, A.; Aird, R. E.; Jodrell, D. I.; Sadler, P. J. *J. Med. Chem.* **2006**, *49*, 6858–6868.
(28) (a) Fish, R. H. *Coord. Chem. Rev.* **1999**, *185−186*, 569–584. (b) Chen, H.; Maestre, M. F.; Fish, R. H. *J. Am. Chem. Soc.* **1995**, *117*, 3631–3632.
(29) Albers, M. O.; Ashworth, T. V.; Oosthuizen, H. E.; Singleton, E. *Inorg. Synth.* **1989**, *26*, 249–258.
(30) Daigle, D. J. *Inorg. Synth.* **1998**, *32*, 40–45.
(31) Dyson, P. J.; McIndoe, J. S. *Inorg. Chim. Acta* **2003**, *354*, 68–74.
(32) Powell, P. *J. Organomet. Chem.* **1974**, *65*, 89–92.

was collected on a frit, washed with diethyl ether (250 mL), and then dried under vacuum overnight. Yield: 3.604 g (88%). Crystals suitable for X-ray diffraction were obtained by slow evaporation of an acetone solution of **1**.

^{1}H NMR (CD_2Cl_2) δ (ppm): 1.91 (s, 6H, CH_3COCH), 1.94−1.99 (m, 2H, C_8H_{12} CH_2), 2.06−2.12 (m, 2H, C_8H_{12} CH_2), 2.16 (s, 6H, CH_3COCH), 2.35−2.44 (m, 4H, C_8H_{12} CH_2), 4.03 (m, 2H, C_8H_{12} C*H*), 4.14 (m, 2H, C_8H_{12} C*H*), 5.34 (s, 1H, CH_3COC*H*), 5.36 (s, 1H, CH_3COC*H*). ^{13}C NMR (CD_2Cl_2) δ (ppm): 27.19 (s, C_8H_{12} CH_2), 27.90 (s, C_8H_{12} CH_2), 28.29 (s, CH_3COCH), 30.12 (s, CH_3COCH), 88.56 (s, C_8H_{12} *C*H), 91.76 (s, C_8H_{12} *C*H), 98.37 (s, CH_3CO*C*H), 185.75 (s, CH_3*C*OCH), 186.50 (s, CH_3*C*OCH).

General Method for the Preparation of 2a−2d. Compounds **2a−2d** were prepared using the method described by Bodes et al.[15] The complex [Ru(η^6-$C_{10}H_8$)(η^4-C_8H_{12})] (1.083 g, 3.2 mM) and the appropriate arene (20 mL, Acros, degassed and dried over 4 Å molecular sieves) were stirred in THF (10 mL, dried and degassed) and MeCN (0.833 g, extra dry quality from Acros) for 7−12 days. The brown solution became slightly lighter in color over time. The solvents were removed under vacuum, and the remaining brown reside was extracted with dried and degassed pentane (25 mL), affording a clear yellow-brown solution. Using a Brockman grade III oxygen-free Al_2O_3 packed column (25 cm × 1 cm) with filter adaptor, the solution was eluted with pentane (80 mL), yielding a bright yellow solution. Volatiles were removed under vacuum, affording a crystalline yellow product, which was dried under vacuum for 2 h. Crystals suitable for X-ray diffraction studies were obtained by slow evaporation of a saturated pentane solution.

[Ru(η^6-C_6H_5F)(η^4-C_8H_{12})], 2a. Yield: 579 mg (66%), yellow powder. ^{1}H NMR (C_6D_6) δ (ppm): 2.38 (m, 8H, C_8H_{12} CH_2), 3.61 (m, 4H, C_8H_{12} C*H*), 4.21 (td, $^3J_{HH}$ = 5.5 Hz, $^3J_{HF}$ = 3.8 Hz, 1H, C_6H_5F *p*-*C*H), 5.15 (dd, $^3J_{HH}$ = 5.5 Hz, $^3J_{HF}$ = 2.7 Hz, 2H, C_6H_5F *o*-CH), 4.74 (dd, $^3J_{HH}$ = 5.5 Hz, $^3J_{HF}$ = 2.7 Hz, 2H, C_6H_5F *m*-*C*H). ^{13}C NMR (C_6D_6) δ (ppm): 31.69 (s, C_8H_{12} *C*H$_2$), 61.35, (s, C_8H_{12} *C*H), 80.79, (s, C_6H_5F *o*-*C*H), 81.16 (s, C_6H_5F *m*-*C*H), 86.13 (s, C_6H_5F *p*-*C*H). ^{19}F NMR (C_6D_6) δ (ppm): −100.01 (*F*-C_6H_5).

[Ru(η^6-$C_6H_5CF_3$)(η^4-C_8H_{12})], 2b . Yield: 932 mg (82%), yellow powder. ^{1}H NMR (C_6D_6) δ (ppm): 2.255−2.397 (m, 8H, C_8H_{12} CH_2), 3.672 (m, 4H, C_8H_{12} C*H*), 4.628 (m, $^3J_{HH}$ = 5.80, 5.92 Hz, 2H, $C_6H_5CF_3$ *m*-*C*H), 4.909 (t, $^3J_{HH}$ = 5.80 Hz, 1H, $C_6H_5CF_3$ *p*-*C*H), 5.101 (d, $^3J_{HH}$ = 5.92 Hz, $C_6H_5CF_3$ *o*-CH). ^{13}C NMR (25 °C, 100.1 MHz, C_6D_6) δ (ppm): 33.69 (s, C_8H_{12} *C*H$_2$), 63.35 (s, C_8H_{12} *C*H), 82.79 (s, $C_6H_5CF_3$ *p*-*C*H), 83.36 (q, $^3J_{CF}$ = 43 Hz, $C_6H_5CF_3$ *o*-*C*H), 86.18 (q, $^1J_{CF}$ = 272 Hz, $C_6H_5CF_3$). ^{19}F NMR (25 °C, 188.1 MHz, C_6D_6) δ (ppm): −60.3 (s, $^1J_{CF}$ = 272 Hz, $C_6H_5CF_3$).

[Ru(η^6-1,4-$CH_3C_6H_4F$)(η^4-C_8H_{12})], 2c . Yield: 73 mg (85%), yellow powder. ^{1}H NMR (C_6D_6) δ (ppm): 1.62 (s, 3H, $CH_3C_6H_5CF$), 2.43 (m, 8H, C_8H_{12} CH_2), 3.50 (m, 4H, C_8H_{12} C*H*), 4.33 (dd, $^3J_{HH}$ = 2.4 Hz, $^4J_{FH}$ = 2.8 Hz, 2H, $CH_3C_6H_4F$ *o*-CH), 5.06 (dd, $^3J_{HH}$ = 2.4 Hz, $^3J_{FH}$ = 2.8 Hz, 2H $CH_3C_6H_4F$ *m*-CH). ^{13}C NMR (C_6D_6) δ (ppm): 17.59 (d, $^5J_{FC}$ = 7.6 Hz, $CH_3C_6H_4F$), 34.06 (s, C_8H_{12} *C*H$_2$), 64.32 (s, C_8H_{12} *C*H), 73.77 (s, $CH_3C_6H_4F$ *o*-*C*H), 82.82 (d, $^3J_{FC}$ = 25.2 Hz, $CH_3C_6H_4F$ *m*-*C*H).

[Ru (η^6-1,4-$C_6H_4F_2$)(η^4-C_8H_{12})], 2d . Yield: 243 mg (43%), yellow powder. ^{1}H NMR (C_6D_6) δ (ppm): 2.26−2.44 (m, 8H, C_8H_{12} CH_2), 3.66 (m, 4H, C_8H_{12} C*H*), 5.31 (d, $^3J_{HF}$ = 5.9 Hz, 1,4-F_2-C_6H_4). ^{13}C NMR (C_6D_6) δ (ppm): 35.23 (s, C_8H_{12} *C*H$_2$), 64.72 (s, C_8H_{12} *C*H), 82.79, 132.6 (s, 1,4-F_2-C_6H_4 *C*H), (s, 1,4-F_2-C_6H_4 *C*F). ^{19}F NMR (C_6D_6) δ (ppm): −138.2 (1,4-*F*$_2$-C_6H_4).

General Method for the Preparation of 3a−3d. To a 50 mL Schlenk flask was added **2** (0.80 mM) under N_2 and dissolved with pentane (15 mL, dried), affording a clear yellow solution. The flask was connected with a Y-tube to a N_2-vacuum line and a HCl gas cylinder with inlet adaptor. After five cycles of purging with N_2 the HCl cylinder was opened, and after 2 min the solution turned red and a precipitate formed. The mixture was stirred for 1 h under N_2 and then filtered (in air) and washed with pentane (100 mL), then Et_2O (25 mL). Finally, CH_2Cl_2 (5 mL, HPLC grade) was added, then Et_2O (10 mL) such that the resulting filtrate was coloress. The orange-red products were dried under vacuum overnight.

[Ru(η^6-C_6H_5F)Cl$_2$]$_2$, 3a. Yield: 540 mg (54%), red powder. ^{1}H (d_6-DMSO) δ (ppm): 5.58 (t, $^3J_{HH}$ = 5.6 Hz, 1H, C_6H_5F *p*-*C*H), 6.12 (dt, $^3J_{HH}$ = 5.6, 5.6 Hz, 2H, C_6H_5F *m*-*C*H), 6.34 (d, 2H, $^3J_{HH}$ = 5.6 Hz, C_6H_5F *o*-CH). ^{13}C NMR (d_6-DMSO) δ (ppm): 70.539 (s, C_6H_5F *o*-CH), 78.59 (s, C_6H_5F *m*-*C*H), 84.37 (s, C_6H_5F *p*-*C*H), 145.88 (s, C_6H_5F *C*F). ^{19}F NMR (d_6-DMSO) δ (ppm): −128 (C_6H_5F).

[Ru(η^6-*C*$_6$H$_5$CF$_3$)Cl$_2$]$_2$, 3b. Yield: 189 mg (74.6%), orange powder. ^{1}H NMR (d_6-DMSO) δ (ppm): 5.91 (dd, $^3J_{HH}$ = 5.6, 5.8 Hz, 2H, $C_6H_5CF_3$ *m*-*C*H), 6.04 (t, $^3J_{HH}$ = 5.6 Hz, 1H, $C_6H_5CF_3$ *p*-*C*H), 6.22 (d, $^3J_{HH}$ = 5.8 Hz, 2H, $C_6H_5CF_3$ *o*-*C*H). ^{19}F NMR (d_6-DMSO) δ (ppm): −61.3 ($C_6H_5CF_3$ C*F*$_3$).

[Ru(η^6-1,4-$CH_3C_6H_4F$)Cl$_2$]$_2$, 3c. Yield: 81 mg (95%), orange powder.

[Ru(η^6-1,4-$C_6H_4F_2$)Cl$_2$]$_2$, 3d. Yield: 121 mg (82.9%), red powder. ^{1}H NMR (d_6-DMSO) δ (ppm): 5.65 (m, $^3J_{HF}$ = 4.8 Hz, 1,4-F_2-C_6H_4). ^{19}F NMR (d_6-DMSO) δ (ppm): −102.4 (1,4-F_2-C_6H_4).

Synthesis of [Ru(η^6-C_6H_5F)Cl$_2$(pta)], 4a. [Ru(η^6-C_6H_5F)Cl$_2$]$_2$ (40 mg, 0.075 mM) and pta (23 mg, 0.15 mM) in CH_2Cl_2 were stirred at RT for 4 h. The product was precipitated by addition of diethyl ether, and the precipitate filtered and washed with diethyl ether (10 mL) and pentane (10 mL). A concentrated solution in H_2O was stored at 4 °C to give crystals suitable for X-ray diffraction. Yield: 32 mg (92%) of pale orange powder.

^{1}H NMR (D_2O) δ (ppm): 4.23 (s, 6H, pta), 4.47 (s, 6H, pta), 5.27 (t, $^3J_{HH}$ = 5.5 Hz, 1H, C_6H_5F *p*-*C*H), 5.84 (d, $^3J_{HH}$ = 5.6 Hz, 2H, C_6H_5F *o*-*C*H), 6.19 (dd, $^3J_{HH}$ = 5.5, 5.6 Hz, 2H, C_6H_5F *m*-*C*H). ^{31}P{^{1}H}NMR (D_2O) δ (ppm): −29.66 (*pta*RuCl$_2$), −28.40 (*pta*RuClH$_2$O). ESI-MS (0.1 M NaCl) *m*/*z* 389.6 [Ru(η^6-C_6H_5F)Cl(pta)]$^+$ (56%), *m*/*z* 424.9 [Ru(η^6-C_6H_5F)Cl$_2$(pta)] (100%), *m*/*z*=448.0 [Ru(η^6-C_6H_5F)Cl$_2$(pta)]Na$^+$ (100%).

Synthesis of [Ru(η^6-$C_6H_5CF_3$)Cl$_2$(pta)], 4b. [Ru(η^6-C_6H_5-CF_3)Cl$_2$]$_2$ (58 mg, 0.09 mM) and pta (28 mg, 0.18 mM) were stirred in CH_2Cl_2. The product formed as a precipitate following several minutes of stirring. The reaction was continued for a further 4 h, and the product was isolated by filtration and then washed with diethyl ether (10 mL) and pentane (10 mL). Yield: 75 mg (92%), orange powder.

^{1}H NMR (D_2O) δ (ppm): 4.234 (s, 6H, pta) 4.47 (s, 6H, pta), 5.82 m, $^3J_{HH}$ = 5.6, 6.2 Hz, 2H, $C_6H_5CF_3$ *m*-*C*H), 5.99 (t, $^3J_{HH}$ = 5.6, 1H, $C_6H_5CF_3$ *p*-*C*H), 6.54 (d, $^3J_{HH}$ = 6.2 Hz, 2H, $C_6H_5CF_3$ *o*-*C*H). ^{31}P{^{1}H} NMR (D_2O) δ (ppm): −30.64. ESI-MS (H_2O) *m*/*z* 474.3 [Ru(η^6-$C_6H_5CF_3$)Cl$_2$(pta-H)]$^+$ (100%).

Synthesis of [Ru(η^6-1,4-$CH_3C_6H_4F$)Cl$_2$(pta)], 4c. [Ru(η^6-1,4-$CH_3C_6H_4F$)Cl$_2$]$_2$ (50 mg, 0.09 mM) and pta (28 mg, 0.18 mM) in CH_2Cl_2 were stirred at RT for 4 h. The product was precipitated by addition of diethyl ether, and the precipitate was filtered and washed with diethyl ether (10 mL) and pentane (10 mL). Vapor diffusion of pentane into a chloroform solution gave crystals suitable for X-ray diffraction. Yield: 68 mg (88%), orange powder.

^{1}H NMR (D_2O) δ (ppm): 1.64 (s, 3H, $CH_3C_6H_4F$), 3.74 (s, 6H, pta), 3.94 (s, 6H, pta) 4.87 (d, $^3J_{HH}$ = 5.2 Hz, 2H, $CH_3C_6H_4F$ *o*-*C*H), 4.96 (d, $^3J_{HH}$ = 5.2 Hz, 2H, $CH_3C_6H_4F$ *m*-*C*H). ^{31}P-{^{1}H}NMR (D_2O) δ (ppm): −32.20. ESI-MS (0.1 M NaCl): *m*/*z* 111.0 C_7H_7F (90%), *m*/*z* 317.7 [RuCl(H$_2$O)(pta)]$^+$Na$^+$ (40%), *m*/*z* 403.9 [Ru(η^6-1,4-$CH_3C_6H_4F$)(OH)(pta)]$^+$ (100%), *m*/*z* 474.3 [Ru(η^6-1,4-$CH_3C_6H_4F$)Cl$_2$(pta)] (70%).

Determination of pK_a Values. The pH values of NMR samples in D_2O were measured at 298 K using a 713 pH meter (Metrohm) equipped with an electrode, which was calibrated with buffer solutions at pH values of 4, 7, and 9. The pH values

were adjusted with dilute HCl and NaOH. The pH titration curves were fitted to the Henderson−Hasselbach equation using the program Micromath Scientist (Micromath Scientist Software Inc.) with the assmption that the observed chemical shifts are weighted averages according to the populations of the protonated and deprotonated species. The resonance frequencies change smoothly with pH between the chemical shifts of the charged form HA^+, stable in acidic solution, and those of the neutral, deprotonated form A, which is present at high pH. At any pH, the observed chemical shift is a weighted average of the two extreme values $\delta(HA^+)$ and $\delta(A)$.

$$\boldsymbol{\delta}_{av} = \frac{\boldsymbol{\delta}(HA^+)[HA^+]+\boldsymbol{\delta}(A)[A^+]}{[HA^+]+[A^+]} \quad (4)$$

The midpoint of the titration occurs when concentration of the acid and its conjugate base are equal: $[HA^+] = [A]$, that is, when the pH equals the pK_a of the compound. The pH at the midpoint of the curve is corrected by subtracting 0.44 from the pD values, as measurements were carried out in D_2O.[33]

DFT Calculations. Calculated pK_a values for the reaction in water, $BH^+_{aq} \rightarrow B_{aq} + H^+_{aq}$, were computed using

$$pK_a = [G(H^+)_{gas}+\Delta G_s(H^+)+G(B)_{gas} + \Delta G_s(B)\ G(BH^+)_{gas} - \Delta G_s(BH^+)]/2.303RT] \quad (5)$$

where $G(X)_{gas}$ denotes the free energy of species X ($X = H^+$, B, BH^+) in the gas phase. $G(X)_{gas}$ is accessible by standard quantum chemical calculations. The computation of $\triangle G_s$-(X), the change in free energy due to solvation of species X, can be performed by using a continuum electrostatic model for the solvent. For derivation of equation 5, the protonation reaction in solution was decomposed into the analogous reaction in the gas phase ($BH^+_{gas} \rightarrow B_{gas} + H^+_{gas}$) as well as into the single solvation reactions of the involved species ($X \rightarrow X_{aq}$). For more details see Liptak et al.[34] Using constant values for $G(H^+)$[34,35] and $\triangle G_s(H)$,[36] eq 5 can be simplified into

$$pK_a = [G(B)_{gas} - G(BH^+)_{gas} + \Delta G_s(B) + \Delta G_s(BH^+) - 269.0]/1.3644 \quad (6)$$

The required quantities were computed at the DFT level employing the B3LYP exchange−correlation functional[36,11] as implemented in the Gaussian03 computer code.[37] Calculations were performed either in the gas phase or using Barone and Cossi's polarizable conducter model for the solvent (C-PCM)[38] to compute $\triangle G_s(X)$.

The zero-point energies, thermal corrections, and entropies obtained from an analytical frequency analysis have been used to convert the internal energies to Gibbs energies at 298.15 K and 1 atm. The same procedure and computational parameters that have been previously used to compute pK_a values of the same class of ruthenium compounds were employed.[11] C-PCM calculations were performed as single points on the gas phase optimized geometries since this has been shown to give better results than reoptimization of the geometries in the presence of the solvent model.[39] Compounds **4a**−**4c** have been found to be stable in different orientations of the arene ligand with respect to the rest of the molecule. The different conformers exhibit large variations in the dipole moments and the solution enthalpies.

Only the pK_a values for the conformers that exhibit the largest solution enthalpies according to the CPCM calculations are reported. In the case of **4a** and **4c**, the conformers with the highest solvation energies are consistent with the determined crystal structures. Water was modeled with a dielectric constant of $\varepsilon = 78.39$. For other C-PCM parameters the default values suggested by Gaussian03 were taken.

A mixed basis set using the quasirelativistic Stuttgart/Dresden semicore SDD-ECP[40] with a (8s7p6d)/[6s5p3d]-GTO triple-ζ valence basis set on ruthenium and 6-31+G(d) on the remaining atoms was used. This method has been shown to yield accurate structures and energies.[41]

X-ray Diffraction Studies. Suitable single crystals were selected and manipulated in a perfluoro-polyalkyl ether oil matrix, and for compounds **2a**−**2d** all operations were performed under a protective blanket of N_2. The crystals were mounted on the end of a glass fiber attached to a metal pin fixed to a goniometer head, which was placed in the Euler cradle, while maintaining a cold blanket of N_2 gas. The data for **2a**, **2b**, and **2d** were collected on a Nonius KappaCDD diffractometer equipped with a Bruker-Apex II CCD area detector and an Enraf-Nonius FR590 X-ray generator. For **1**, **4a**, and **4c**, an Oxford-Kuma Kappa diffractometer with a Sapphire CCD area detector and for **2c**, a Marresearch mardtb desktop goniostat with a Mar345 image plate were employed. All instruments utilize a graphite-monochromatic Mo Kα radiation source with $\lambda = 0.71073$ Å. The crystals were kept under a 140 or 100 K gaseous flow of N_2 during data collection. For **2a**, **2b**, and **2d** the unit cell and orientation matrix was determined by indexing reflections measured from phi-chi scans and analyzed with the program DIRAX,[42] while for the remaining structures, the unit cells were determined from the entire data set using CrysAlis RED.[43] All data sets are based on collecting reflections using an optimized scanning strategy utilizing the programs CollectCCD,[44] CrysAlis CCD, or autoMar.[45] After data integration with either EvalCCD[46] or CrysAlis RED, a multiscan absorption correction based on a semiempirical method was applied using the SADABS,[47] ABSPACK (a subprogram of the CrysAlis RED). Space group determination was performed with the XPREP program.[48] A structure solution based on the direct-method algorithm was employed with SHELXS-97.[49] Afterward, anisotropic refinement of all non-hydrogen atoms was completed based on a least-squares full-matrix method against F^2

(33) Mikkelesen, K.; Nielsen, S. O. *J. Phys. Chem.* **1960**, *64*, 632–637.
(34) Liptak, M. D.; Gross, K. C.; Seybold, P. G.; Feldgus, S.; Shields, G. C. *J. Am. Chem. Soc.* **2002**, *124*, 6421–6427.
(35) McQuarrie, D. M. *Statistical Mechanics*; Harper and Row: New York, 1970.
(36) Becke, A. D. *J. Chem. Phys.* **1993**, *98*, 5648–5652.
(37) *Gaussian 03*, Revision B.03; Gaussian, Inc.: Wallingford, CT, 2004.
(38) (a) Barone, V.; Cossi, M. *J. Phys. Chem. A* **1998**, *102*, 1995–2001. (b) Cossi, M.; Rega, N.; Scalmani, G.; Barone, V. *J. Comput. Chem.* **2003**, *24*, 669–681.
(39) Halvani, S.; Noorbala, M. R. *THEOCHEM* **2004**, *711*, 13–18.
(40) Andrae, D.; Haeussermann, U.; Dolg, M.; Stoll, H.; Preuss, H. *Theor. Chim. Acta* **1990**, *77*, 123–41.
(41) (a) Dorcier, A.; Dyson, P. J.; Gossens, C.; Rothlisberger, U.; Scopelliti, R.; Tavernelli, I. *Organometallics* **2005**, *24*, 2114–2123. (b) Kallies, B.; Mitzner, R. J. *Phys. Chem. B* **1997**, *101*, 2959–2967. (c) De Abreu, H. A.; De Almeida, W. B.; Duarte, H. A. *Chem. Phys. Lett.* **2004**, *383*, 47–52.
(42) Duisenberg, A. J. M. *J. Appl. Crystallogr.* **1992**, *25*, 92–96.
(43) *CrysAlis CCD and CrysAlis RED, version 1.71*; Oxford Diffraction Ltd: Abingdon, 2006.
(44) *COLLECT: data collection software*; Bruker AXIS B.V.: Delft, 1999.
(45) *Automar, version 1.8*; Marresearch G.m.b.H.: Norderstedt, 2005.
(46) Duisenberg, A. J. M.; Kroon-Batenburg, L. M. J.; Schreurs, A. M. M. *J. Appl. Crystallogr.* **2003**, *36*, 220–229.
(47) Sheldrick, G. M. *SADABS: Area detector absorption and other corrections, version 2.06*; Bruker-AXS: Madison, 2003.
(48) *XPREP: Reciprocal Space Exploration, version 6.14*; Bruker-AXS: Madison, 2003.
(49) Sheldrick, G. M. *SHELXS-97, Program for Crystal Structure Solution*; University Göttingen: Germany, 1997.

Table 7. Selected Crystallographic Data for 1, 2a, 2b, and 2c

parameter	1	2a	2b	2c
formula	$C_{18}H_{26}O_4Ru$	$C_{14}H_{17}F_1Ru$	$C_{15}H_{17}F_3Ru$	$C_{15}H_{19}F_1Ru$
fw (g mol^{-1})	407.46	305.35	355.36	319.37
cryst syst	monoclinic	monoclinic	orthorhombic	monoclinic
space group	$P2_1/n$	$C2/c$	$P2_12_12_1$	$P2_1/c$
a (Å)	7.7873(3)	23.552(5)	8.2277(16)	12.377(3)
b (Å)	16.0694(4)	8.1761(16)	11.069(7)	8.3601(10)
c (Å)	14.4680(4)	24.319(5)	14.291(3)	12.819(3)
α (deg)	90	90	90	90
β (deg)	104.012(3)	101.82(3)	90	109.621(18)
γ (deg)	90	90	90	90
volume (Å^3)	1756.61(10)	4583.5(16)	1301.5(4)	1249.4(5)
Z	4	16	4	4
D_{calc} (g cm^{-3})	1.541	1.770	1.814	1.698
μ (mm^{-1})	0.909	1.349	1.222	1.241
$F(000)$	840	2464	712	648
temp (K)	140(2)	100(2)	100(2)	140(2)
measd reflns	10 241	44 739	24977	7274
unique reflns	2986	4025	2286	2197
theta range (deg)/completeness (%)	2.90 to 25.00/96.5	3.42 to 25.00/99.8	3.39 to 25.00/99.7	2.96 to 24.99/99.9
no. of data/ params/restraints	2986/212/0	4025/309/66	2286/172/0	2197/164/0
GooF[a]	1.016	1.505	1.079	1.152
R**b** [$I > 2\sigma(I)$]	0.0249	0.351	0.0126	0.0280
wR_2[b] (all data)	0.0652	0.836	0.0296	0.0724
largest diff peak/hole (e Å^{-3})	0.959/−0.427	0.789/−1.096	0.198/−0.236	1.035 and −0.742

[a] GooF is defined as $\{\sum[w(F_o^2 - F_c^2)^2]/(n-p)\}^{1/2}$ where n is the number of data and p is the number of parameters refined. [b] $R = \sum||F_o| - |F_c||/\sum|F_o|$, $wR_2 = \{\sum[w(F_o^2 - F_c^2)^2]/\sum[w(F_o^2)^2]\}^{1/2}$.

Table 8. Selected Crystallographic Data for 2d, 4a, and 4c

parameter	2d	4a	4c
formula	$C_{14}H_{16}F_2Ru$	$C_{12}H_{22}Cl_2F_1N_3O_{2.50}P_1Ru$	$C_{13}H_{19}Cl_2F_1N_3P_1Ru$
fw (g mol^{-1})	323.34	470.27	439.25
cryst syst	orthorhombic	monoclinic	triclinic
space group	$P2_12_12_1$	$P2_1/c$	$P\bar{1}$
a (Å)	6.4319(5)	9.4040(2)	7.0518(3)
b (Å)	7.6925(7)	15.7312(3)	10.8932(5)
c (Å)	23.9146(19)	11.9961(4)	10.9145(5)
α (deg)	90	90	110.878(4)
β (deg)	90	105.972(3)	94.109(3)
γ (deg)	90	90	94.542(3)
volume (Å^3)	1183.23(19)	1706.15(8)	776.40(6)
Z	4	4	2
D_{calc} (g cm^{-3})	1.815	1.831	1.879
μ (mm^{-1})	1.323	1.348	1.463
$F(000)$	648	948	440
temp (K)	100(2)	140(2)	140(2)
measd reflns	15694	9689	4639
unique reflns	1078	2671	2346
theta range (deg)/completeness (%)	3.41 to 25.00/99.6	2.77 to 25.00/88.8	3.32 to 25.00/86.4
no. of data/ params/restraints	2078/156/0	2671/237/4	2346/191/0
GooF[a]	1.097	1.054	1.053
R[b] [$I > 2\sigma(I)$]	0.0200	0.0210	0.0150
wR_2[b] (all data)	0.0489	0.0616	0.0392
largest diff peak/hole (e Å^{-3})	0.334/−1.263	0.695/−0.546	0.243/−0.307

[a] GooF is defined as $\{\sum[w(F_o^2 - F_c^2)^2]/(n-p)\}^{1/2}$ where n is the number of data and p is the number of parameters refined. [b] $R = \sum||F_o| - |F_c||/\sum|F_o|$, $wR_2 = \{\sum[w(F_o^2 - F_c^2)^2]/\sum[w(F_o^2)^2]\}^{1/2}$.

data using SHELXL-97.[50] Hydrogen atoms were added in geometrically calculated positions and refined as a riding model using a scaled thermal parameter to the connecting atom. In **2a** and **2c**, positional disordering of the fluorine and methyl group (**2c** only) was observed and resolved by splitting the atoms over two positions and allowing the total occupancy of the disordered groups to freely refine. For structure **4a**, a number of disordered water molecules were observed. The total occupancy for all of the water molecules was restricted to a total of 2.5 units, which is in accordance with the number of electrons associated with the solvate region. Hydrogen atoms that belong to the water were located on the electron density difference map, and the H−O bond lengths and the H−O−H bond angles were constrained to reasonable values. Where possible, suitable hydrogen acceptors were located using the program Calc-OH[51] and the H−O vectors positioned to form hydrogen-bonding interactions. The coordinates of the hydrogen atoms belonging to water were allowed to freely refine with the thermal parameter set to a scaled value of the associated oxygen atom. A small number of reflections (in some cases) were removed when

(50) Sheldrick, G. M. *SHELXL-97, Program for Crystal Structure Refinement*; University Göttingen: Germany, 1997.

(51) Nardelli, M. *J. Appl. Crystallogr.* **1999**, *32*, 563–571.

$\Delta(F_o^2-F_c^2)/\sigma$ exceeded 10.0. Key data for all structures are given in Tables 7 and 8. Drawings in Figures 3 through 5 were produced with the program Diamond 3.1e.[52]

Cell Line and Culture Conditions. The human A2780 ovarian cancer cell line was obtained from the European Collection of Cell Cultures (Salisbury, UK). Cells were grown routinely in RPMI medium containing glucose, 5% fetal calf serum (FCS), and antibiotics at 37 °C and 5% CO_2.

Cytotoxicity Test (MTT assay). Cytotoxicity was determined using the MTT assay (MTT = 3-(4,5-dimethyl-2-thiazolyl)-2,5-diphenyl-2*H*-tetrazolium bromide). Cells were seeded in 96-well plates as monolayers with 100 μL of cell solution (approximately 20 000 cells) per well and preincubated for 24 h in medium supplemeted with 10% FCS. Compounds were dissolved directly in the culture medium, with the exception of **4b**, which was added as a DMSO solution, and serially diluted to the appropriate concentration (final DMSO concentration = 0.5%). Then 100 μL of drug solution was added to each well and the plates were incubated for another 72 h. Subsequently, MTT (5 mg/mL solution in phosphate-buffered saline) was added to the cells, and the plates were incubated for a further 2 h. The culture medium was aspirated, and the purple formazan crystals formed by the mitochondrial dehydrogenase activity of vital cells were dissolved in DMSO. The optical density, directly proportional to the number of surviving cells, was quantified at 540 nm using a multiwell plate reader, and the fraction of surviving cells was calculated from the absorbance of untreated control cells. Evaluation is based on means from two independent experiments, each comprising three microcultures per concentration level.

(52) *Diamond: Crystal and Molecular Structure Visualization, version 3.1e*; Crystal Impact: Bonn, 2007.

Acknowledgment. We thank the Swiss National Science Foundation and EPFL for financial support. This research was also supported by a grant from the European Commission Marie Curie Action (ADP, Project CARCAS, MEIF-CT-2005-025287).

Supporting Information Available: CIF files giving crystallographic data for **1**, **2a**−**d**, **4a**, and **4c**. This material is available free of charge via the Internet at http://pubs.acs.org.